ESTIMATING THE NUMBER OF ACTIVE DEVICES WITHIN A FIXED AREA USING WI-FI MONITORING

A Thesis

by

HAI LI

Submitted to the Office of Graduate and Professional Studies of
Texas A&M University
in partial fulfillment of the requirement for the degree of

MASTER OF SCIENCE

Chair of Committee,	Jean-Francois Chamberland
Committee Members,	Gregory H. Huff
	Anxiao Jiang
	Tie Liu
Head of Department,	Jose Silva-Martinez

December 2016

Major Subject: Electrical and Computer Engineering

ABSTRACT

In various situations, there is a need to estimate the number of active devices within a specific area. This thesis offers one possible approach to accomplish this task. It focuses on estimating the number of devices in a certain area based on monitoring and processing Wi-Fi metadata which includes the Received Signal Strength Indicator. To accomplish this goal, four sensing devices are placed at the corners of a rectangular area. These sensing devices observe and record local data traffic, along with the received signal strength associated with each packets. For each sensing device, two types of frontends are considered, namely directional and isotropic antennas. Each sensing device retrieves the received signal strength indicators and the media access control addresses from the 802.11 frames packets transmitted by nearby active wireless devices. The estimator takes the received signal strength indicators as input and infers the number of active Wi-Fi devices inside the area of interest. Two algorithms, bayesian and maximum-likelihood, are employed for estimation purposes. Overall performance is used to compare and contrast the systems implemented with directional antennas and isotropic antennas, respectively. Theoretical and experimental results both hint at performance improvements when using directional antennas, when compare to standard isotropic antennas.

This dissertation work is dedicated to my advisors - Dr. J.F.Chamberland, my father, my mother, my friends for their support through out the process.

ACKNOWLEDGMENTS

I would like to express gratitude to my advisor, Dr. Jean-Francois Chamberland, for his guidance throughout this research. His continuous support makes this project a success. My sincere thanks to Dr. Gregory Huff. I am grateful to his team at the Wireless Communications Laboratory for providing the antennas we used through out the experiment. I am grateful to my rest committee members, Dr. Tie Liu, Dr. Anxiao Jiang for their expert evaluation and feedback. I would also like to thank the faculty and staff of the Department of Electrical Engineering at Texas A&M University.

I am grateful to my lab mates- Pranay Kumar, Naga Raghave Anudeep, Nagaraj, Travis Taghavi, Austin Taghavi, Mandel Oats and Derek Heidtke for for their feedback and support in all phases of the project.

I wish to express my gratitude to my friends and colleagues for making my time at Texas A&M University a great experience. Last I want to thank my family, who have always supported me.

NOMENCLATURE

RSSI	Received Signal Strength Indicator
MAC	Media Access Control
NUC	Intel’s Next Unit of Computing device
BMSE	Bayesian Mean Square Error
MSE	Mean Square Error

TABLE OF CONTENTS

Page

ABSTRACT ii

DEDICATION iii

ACKNOWLEDGMENTS iv

NOMENCLATURE v

TABLE OF CONTENTS vi

LIST OF FIGURES viii

LIST OF TABLES xi

1 INTRODUCTION 1

1.1 The Wireless Environment 2

2 SYSTEM MODEL AND PROBLEM FORMULATION 8

2.1 Wireless Channel Model 8
2.2 Problem Formulation 10

3 ESTIMATION SCHEMES 14

3.1 Bayes Estimation 14
3.2 Maximum likelihood estimation 16

4 NUMERICAL SIMULATION SETUP AND RESULTS 19

4.1 Antenna Characteristic 19
4.2 Channel Characteristic 20
4.3 Generating Data Set 21
4.4 Performance Analysis 22
4.4.1 Bayes Estimation 22

4.4.2 Maximum Likelihood Estimation 26

5 EXPERIMENTAL IMPLEMENTATION 30

5.1 Monitoring Devices 30
5.2 Wireless client 31
5.3 Experimental Samples 32
5.4 Channel Parameters 33
5.5 Experiment Results 33
5.5.1 Performance of Bayes Estimation 33
5.5.2 Performance of Maximum Estimation 37

6 CONCLUSION 40

REFERENCES 41

LIST OF FIGURES

FIGURE Page

2.1 The periphery of target area is delineated by the dashed line. Squares at the corners of target area denote the locations of the monitoring devices, equipped with directional antennas. Clients within the zone of interest are in black, whereas outside agents appear in white. The objective is to estimate occupancy within target area. 11

4.1 This graph depicts normalized antenna radiation patterns. The pointing direction is set to 0° and $G_{\text{floor}} = 20$ dB. 20

4.2 This graph shows Bayesian mean squared error as functions of splitting parameter under scheme of 3.1. Black line correspond to performance of system equipped with isotropic antennas, whereas red line correspond to the performance of systems with directional antennas. 24

4.3 This graph shows the approximation probability density function of $|r_t - \hat{r}_t|$ corresponding to system equipped with directional antennas under the scheme of Section 3.1. 26

4.4 This graph shows the approximation probability density function of $|r_t - \hat{r}_t|$ corresponding to system equipped with isotropic antennas under scheme of 3.1. 27

4.5 This figure shows mean squared error as functions of splitting parameter under scheme of Section 3.2. Black line correspond to performance of system equipped with isotropic antennas, whereas red line correspond to the performance of systems with directional antennas. 27

4.6 This graph shows the approximation probability density function of $|r_t - \hat{r}_t|$ corresponding to system equipped with directional antennas under scheme of 3.2. 29

4.7 This graph shows the approximation probability density function of $|r_t - \hat{r}_t|$ corresponding to system equipped with isotropic antennas under scheme of 3.2. 29

5.1 This graph depicts directional antenna radiation patterns 31

5.2 This graph shows the monitoring device we use. 32

5.3 This figure highlights the site used for the experiments and marks locations of experiment data. 34

5.4 This figure depicts the experimental Bayesian mean squared error as function of Poisson splitting coefficient α. Red line represents systems with directional antennas, whereas black line represent system with isotropic antennas. 35

5.5 This graph shows the approximation probability density function of $|r_t - \hat{r}_t|$ corresponding to system equipped with directional antennas under scheme of 3.1. 36

5.6 This graph shows the approximation probability density function of $|r_t - \hat{r}_t|$ corresponding to system equipped with isotropic antennas under scheme of 3.1. 36

5.7 This figure depicts the experimental Bayesian mean squared error as function of Poisson splitting coefficient α. Red line represents systems with directional antennas, whereas black line represent system with isotropic antennas. 37

5.8 This graph shows the approximation probability density function of $|r_t - \hat{r}_t|$ corresponding to system equipped with directional antennas under scheme of 3.2. 38

5.9 This graph shows the approximation probability density function of $|r_t - \hat{r}_t|$ corresponding to system equipped with isotropic antennas under scheme of 3.2. 38

LIST OF TABLES

TABLE		Page
4.1	System parameters used during simulations.	21
4.2	Confidence interval of $\lvert r_t - \hat{r}_t \rvert$ for simulation Bayes scheme	25
4.3	Confidence interval of $\lvert r_t - \hat{r}_t \rvert$ for simulation corresponding to the Maximum likelihood scheme.	28
5.1	Confidence interval of $\lvert r_t - \hat{r}_t \rvert$ for experimental Bayes scheme	35
5.2	Confidence interval of $\lvert r_t - \hat{r}_t \rvert$ for experimental Maximum estimation scheme	37

1 INTRODUCTION

Occupancy estimation refers to the problem to estimate the number of people inside a certain area. This topic has attracted lots of interests for years due to its importance. There are several potential applications that can benefit from occupancy estimation. In smart building automation systems, using knowledge of the level of occupancy, it is possible to optimize the energy cost over the control of temperature and ventilation. This can result in a large amount of energy saving [1, 2]. In navigation systems, providing road occupancy traffic information will allow users to find out the best route to the destination. In [3], the author proposed a road monitoring system that encompass UMTS and GPRS data collection. Under an emergency circumstance, a proper occupancy estimation may help the government guide the evacuation of crowds.

In recent years, the number of Wi-Fi access points and the number of Wi-Fi client devices have been increasing dramatically. This growth in Wi-Fi infrastructure leads to large amounts of data being transmitted over wireless networks. Cisco Systems predicts in their Visual Network Index that 55 percent of total mobile data traffic will be offloaded onto fixed networks through Wi-Fi access points and femtocells by 2020 [4]. This means Wi-Fi is increasingly becoming a prime data source since Wi-Fi signals can tell us about our environment. A lot of attention is drawn into this area, with topics such as self-localization, source localization and occupancy estimation [5, 6].

At the same time, we have witnessed the rapid development of mobile technology

which is fuelled by a large amount of smartphone users. Smartphone supports real-time communication and information access, with an advanced mobile operating system that combines features of a personal computer and other features useful for mobile use. Smartphones are influencing human activity significantly. The global smartphone penetration rate has grown fast over past years. According to eMarketer's prediction in [7], smartphone user penetration as percentage of total global population will be 34.64 percent by 2019. In the U.S., 197.4 million people owned smartphones (79.3 percent mobile market penetration) during the three months ending in December 2015 according to comScore's report [8]. This rapid development demands an improved manufacturing process. As the result, mass production involved in smartphone technology have decreased the cost of smartphone components. This fact makes smartphones prize-friendly to users. Notably smartphone operation systems also play important roles in mobile devices. For instance, Android system provides the manufacturer a tool to produce multi-platform application for smartphone. This makes the development procedure cheaper and it gets devices in the hands of more people. Overall, the continuous growth in mobile technology attracts more attention into this field.

1.1 The Wireless Environment

In this work, we are interested in the occupancy estimation based on Wi-Fi activity of the users. A good understanding of the wireless channel is key to analyze communication systems. With this in mind, we will discuss important concepts in channel modeling

like path loss, shadow fading and multipath propagation. Path loss refers to the attenuation in the transmitted signal while propagating from the transmitter (Tx) to the receiver (Rx). Received signal power is a function of the distance between Tx and Rx. The simplest path loss model is used for unobstructed line-of-sight (LOS) signal path in free space propagation. Under this model, the received signal is given by

$$P_R = P_T G_T G_R \frac{\lambda^2}{4\pi d^2} \tag{1.1}$$

where P_T is the transmitted power, G_T and G_R are the transmit and receive antenna gains, respectively, λ is the transmitted carrier wavelength, and d is the distance between Tx and Rx. Thus, the received power falls off proportional to the ratio of wavelength over distance squared. This also establishes the relation between path loss and wave length: shorter wave length, higher path loss. Though simple, the free space path loss model cannot be accurate in real environments. Therefore, we need to take more factors into consideration.

In the previous path loss model, we assume the path loss to be a constant if the distance is given. However in reality, the presence of obstacles like buildings and trees between transmitter and receiver may bring random variations in path loss. This effect is due to changes in scattering, reflecting and diffracting surfaces in the propagation environment and it is called shadowing [9]. Considering shadowing, the received signal power becomes

$$P_R = P_T G_T G_R S \tag{1.2}$$

where P_L and S correspond to the path loss and the shadow fading factor,respectively. Above, S is a random variable. Experiment results show that a log-normal distribution function provides a good match to the empirical pdf of the shadow fading component [10].

Therefore, the pdf of S can be approximated as the pdf of a Gaussian random variable when S is expressed in dB domain.

$$f_{S_s}(s) = \frac{1}{\sqrt{2\pi}\sigma_s} \exp\left(-\frac{s^2}{2\sigma_s^2}\right) \tag{1.3}$$

where σ_s is the standard deviation of shadowing. Typically σ_s is between 5-10 dB.

Multipath fading occurs as a result of the transmitted signal reflection, diffraction, and/or scattering on objects before reaching the destination. Multiple copies of the signal may arrive at different phases. Multipath fading may also cause inter-symbol interference. Compared with shadowing fading, multipath fading is a short-term factor that generally causes smaller effects to the signal power. Therefore, the multipath fading is also called small-scale fading. Some model such as Rayleigh fading and Ricean fading can be used for multipath fading [9]. Rayleigh fading is a reasonable model when there are many objects in the environment that scatter the radio signal before it arrives at the receiver. However, when a LOS exists or a strong reflected path, termed specular component, also arrives at the receiver, the fading is more appropriately modeled by a Rician distribution [11]. Several different models such as Okumura, Hata, Walfish-Ikegami have been proposed to model different environments like urban, rural and indoor areas [11].

Current literature on occupancy estimation is largely based on either images or RF signals. Approaches based on cameras use captured images to estimate the number of people in a crowded scene [12, 13, 14]. Still, in such camera-based approaches, estimation accuracy can be affected by many factors such as brightness and image resolution. In addition, camera-based approaches typically lead to high deployment cost, which makes it

inconvenient to deploy in reality. On the other hand, occupancy estimation based on RF signals is more promising. This category encompasses several methods. Passive infrared sensor is one of the common technologies used in the past few years. In [15], they proposed an occupancy estimation system which is able to adjust with movement of the people inside the building. The author shows that about 5% more energy can be saved by using smart occupancy sensor as compared to non-adapting fixed time-delay sensors. In [16], an indoor occupancy estimation using ultrasonic chirps is proposed. The author shows that the average error in percentage to the maximum capacity of the room is around 5%. However, this option is an active sensing system; if multiple transducers are placed in the same room, each transducer will interfere with others. Some other methods involved Bluetooth [17] and Wi-Fi [18]. However, the short transmission range limits the performance of Bluetooth-based methods. A research compared Wi-Fi and Bluetooth approaches [19]. In their work, the authors stipulate that Wi-Fi has advantage over Bluetooth in monitoring people, due to shorter discovery time and higher detection rates. According to their results, more than 90% of scanned unique MAC addresses in all places are Wi-Fi addresses; the popularity of using Wi-Fi devices is therefore significantly higher than that of Bluetooth devices, which means occupancy estimation using Wi-Fi is much more convenient in practice. In [20], the author proposes FCC, a device-Free Crowd Counting approach based on channel state information measurements. In [21], the author develops a new approach for estimating the total number of people walking in an area with only Wi-Fi power measurements between a pair of stationary transmitter/receiver antennas. In that case, they do not

need the measurement of channel state information.

In this thesis, we are interested in estimating the number of active devices in a fixed area using Wi-Fi metadata. Modern mobile devices equipped with Wi-Fi modules transmit Wi-Fi messages periodically. Therefore, this provides a means to estimate occupancy by passively listening to Wi-Fi packets. More specifically, by deploying Wi-Fi monitoring devices in an area of interest, it is possible to detect these Wi-Fi transmissions. Each acquired Wi-Fi packet contains a unique MAC address. This information can be augmented by the received signal strength indicator (RSSI) of the captured signal. In the current context, the MAC address serves as a device identifier, whereas the RSSI provides partial information about the physical distance between the transmitter and the receiver. This information is helpful in inferring the device location status. The existence of `pcap`, an application programming interface for capturing network traffic, and wireshark, a network protocol analyzer, makes the Wi-Fi traffic analysis straightforward.

In the research, we focus on occupancy estimation based on Wi-Fi packets and we analyze the benefits associated with using directional antennas. On the one hand, we are going to introduce two stochastic estimation schemes. One is a Bayes estimation scheme and the other is a maximum likelihood scheme. On the other hand, we will investigate the benefit by using directional antennas in monitoring devices. Because the radiation pattern of antenna will influence the RF propagation, it is naturally to think of the potential impacts it brings to use directional antennas. We employ numerical simulations to compare the performance of different schemes corresponding to sensing devices with directional

antennas and isotropic antennas. In the simulation, we assume that four sensing devices are located in the four corners of a rectangular target area. The training RSSI values are assumed to obey free-space path loss model as well. Our results indicate if directional antennas are used, the error rate decreases considerably. In addition, our findings are further supported through outdoor experimentation. The testbed is implemented in a line-of-sight environment, with four sensing devices deployed at the corners of the area of interest.

The remainder of this thesis is organized as follows. In Section 2, we explain our problem formulation and develop a probability model. In Section 3, we propose two algorithms for occupancy estimation. These schemes are evaluated through numerical simulations in Section 4. We then discuss experimental results, along with description of experiment setup in Section 5. Finally, we offer concluding remarks in Section 6.

2 SYSTEM MODEL AND PROBLEM FORMULATION

Wi-Fi based occupancy estimation is attractive because it only require simple sensing devices. Meanwhile, it can benefit from local Wi-Fi network and the high penetration rate of smartphones. The existence of tools like `pcap` and wireshark makes monitoring Wi-Fi environments a straightforward task. In this thesis, we extract the RSSI and MAC address for the purpose of occupancy estimation. As discussed above, the RSSI is related to the distance between the Rx and Tx. Therefore, we can estimate the location information based on RSSI values. However, RSSI does not depend only on distance; some other factors like noise and fading can also influence it. As such, a proper wireless channel model is needed to take care of this situation.

2.1 Wireless Channel Model

A common wireless environment can be express by

$$r(t) = g(d)s(t) + w(t)$$

where $r(t)$ represents received signal; the function $g(d)$ is the power gain which is related to several factors including the mean path loss, shadow fading and antenna gain; $s(t)$ denotes the sent signal; and $w(t)$ is additive white Gaussian noise. Herein, we adopt the log-normal channel model. So, the received power for a given distance between transmitter and receiver can be expressed as

$$P_d[\text{dBm}] = A + B\log_{10}(d) + L_s + G_a \tag{2.1}$$

where A is a combination of the transmitted signal power and average path loss and B represents the path loss coefficient. Component L_s is a Gaussian random variable that captures shadowing. Finally, G_a is the antenna gain. We note that the mean of L_s can be added in A; thus, we assume L_s is a zero mean random variable, $L_s \sim \mathcal{N}(0, \sigma_s^2)$. Parameter σ_s is the variance of shadowing component. In the logarithmic domain, the probability density function of L_s can be written as

$$f_{L_s}(\ell) = \frac{1}{\sqrt{2\pi}\sigma_s} \exp\left(-\frac{\ell^2}{2\sigma_s^2}\right).$$

Here the variance can be estimated by sample data set. An unbiased estimator for the variance is given by [22]

$$\sigma_s^2 = \frac{1}{N-1} \sum_{1}^{N} (l_k - \mu_s)^2$$

where N is the sample size, l_k forms the data set, and points are expressed in the logarithmic domain [23, 24].

In a practical setting, we need to estimate the wireless channel parameters A and B. To do so, we use the method of least squares, which minimizes the sum of the squares of the offsets. Consider the linear least squares problem given by

$$f(x, \beta) = \sum_{j=1}^{m} \beta_j \phi_j(x)$$

where ϕ_j is a function of x and β is the parameter vector to be estimated. Letting matrix M be defined by

$$M_{ij} = \frac{\partial f(x_i, \beta)}{\partial \beta_j} = \phi_j(x_i),$$

the least squares estimate for β becomes

$$\hat{\beta} = (M^T M)^{-1} M^T \mathbf{y}.$$

For the least square problem defined in Section 2.1, we let

$$\mathbf{y} = \begin{bmatrix} p_1 \\ \vdots \\ p_N \end{bmatrix} \qquad M = \begin{bmatrix} 1 & \log_{10}(d_1) \\ \vdots & \vdots \\ 1 & \log_{10}(d_N) \end{bmatrix}$$

where $\mathbf{y}$ denotes the received power at distance d. Then, the estimator of A and B is given as

$$\begin{bmatrix} A \\ B \end{bmatrix} = (M^T M)^{-1} M^T \mathbf{y}.$$

The variance of L_s, the shadow fading component, is computed by normalizing the residual error

$$\sigma_s^2 = \frac{1}{N-1} \mathbf{y}^T (I - M(M^T M)^{-1} M^T) \mathbf{y}.$$

2.2 Problem Formulation

Consider a scenario where several wireless devices are randomly positioned nearby an area of interest. To simplify the problem, we assume the area to be rectangular shape. Four RF monitoring devices are located at the corners of this region. Each monitoring device has information concerning its own location and orientation. The radiation pattern of the antenna attached to each monitoring device is known as well. In our system model, all of the monitoring devices are connected to the Internet and send the captured data to a process center for inference. Several wireless clients carried by users are randomly located

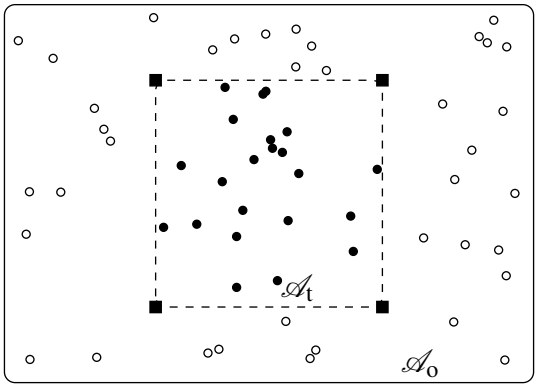

Figure 2.1: The periphery of target area is delineated by the dashed line. Squares at the corners of target area denote the locations of the monitoring devices, equipped with directional antennas. Clients within the zone of interest are in black, whereas outside agents appear in white. The objective is to estimate occupancy within target area.

near this area, they can be inside or outside the area of interest. The wireless clients transmit data packets periodically and, consequently, they can be easily detected by the monitoring devices. Since each wireless client has a unique MAC address, the packets transmitted from different clients can be distinguished. Throughout, we use $\mathscr{A}_t$ to represent the target area and $\mathscr{A}_o$ to represent its complement. A notional diagram of the framework is shown in Fig. 2.1

In this thesis, we assume the wireless clients are quasi-static and each client is equipped with an isotropic antenna. Thus, the orientation of the wireless clients does not matter. For convenience, we use a single vector to denote the locations of the wireless clients.

$$\underline{\mathbf{U}} = (\mathbf{U}_1, \ldots, \mathbf{U}_{n_a}) \tag{2.2}$$

where n_a is the number of the detected clients. We also assume that the signal captured by a monitoring device comes from a line-of-sight path. Therefore, signal strength subscribes

to a free-space transmission model. The received signal strength from client j to sensing device i can be expressed using the log-normal channel model,

$$P_{ij}[\text{dBm}] = A + B\log_{10}(d_{ij}) + L_{ij} + G_i(\phi_{ij}) \tag{2.3}$$

where A and B are the mean decay parameters, d_{ij} is the Euclidean distance between the client j and sensing device i. This distance is equal to

$$d_{ij} = d(\mathbf{s}_i, \mathbf{u}_j) = \sqrt{(u_{1j} - s_{1i})^2 + (u_{2j} - s_{2i})^2}.$$

Variable L_{ij} represent shadow fading and parameter $G_i(\cdot)$ is the antenna gain function of the sensing device. Parameter ϕ_{ij} denotes the angle of the signal transmission direction, which can be expressed as

$$\phi_{ij} = \angle(\mathbf{s}_i, \mathbf{u}_j) = \text{atan2}(u_{2j} - s_{2i}, u_{1j} - s_{1i}).$$

The shadow fading components $\{L_{ij}\}$ are assumed to be independent and identically log-normal distributed random variables. In the logarithmic domain, the probability density function is

$$f_{L_{ij}}(\ell) = \frac{1}{\sqrt{2\pi}\sigma_{\text{s}}} \exp\left(-\frac{\ell^2}{2\sigma_{\text{s}}^2}\right), \tag{2.4}$$

where σ_{s} is the standard deviation of shadowing.

The observed information from the four sensing devices form a power matrix $\underline{\mathbf{P}} = (\mathbf{P}_1, \ldots, \mathbf{P}_{n_{\text{a}}})$. The vector element $\mathbf{P}_j = (P_{1j}, P_{2j}, P_{3j}, P_{4j})$ contains the signal strength of the wireless client j detected by four sensing devices. We assume the number and locations of the wireless clients located inside the area of interest form a Poisson point process with intensity λ_{t}. Therefore, the probability that r_t wireless clients lie inside the target area is

equal to

$$\Pr(R_{\mathrm{t}} = r_{\mathrm{t}}) = \frac{(\lambda_{\mathrm{t}} A_{\mathrm{t}})^{r_{\mathrm{t}}}}{r_{\mathrm{t}}!} e^{-A_{\mathrm{t}}\lambda_{\mathrm{t}}} \quad r_{\mathrm{t}} = 0, 1, \ldots$$

where R_{t} is the number of clients inside and A_{t} is the area of the target region. Similarly, we can write the probability that r_o wireless clients are located outside the target area as

$$\Pr(R_{\mathrm{o}} = r_{\mathrm{o}}) = \frac{(\lambda_{\mathrm{o}} A_{\mathrm{o}})^{r_{\mathrm{o}}}}{r_{\mathrm{o}}!} e^{-A_{\mathrm{o}}\lambda_{\mathrm{o}}} \quad r_{\mathrm{o}} = 0, 1, \ldots$$

where R_{o} is the number of clients outside, A_{o} is the area of the complimentary of target region, and λ_{o} is a Poisson intensity parameter. The inference task is to estimate occupancy based on the power matrix data set $\underline{\mathbf{P}}$ which is collected by the sensing devices.

3 ESTIMATION SCHEMES

In this section, we introduce the two estimation schemes employed in this thesis. A Bayes estimation scheme and a maximum likelihood estimation algorithm are considered and they are applied under different scenarios. If the estimation process is applied repetitively over time, then acquired data can be employed to gain accurate estimates for λ_t and λ_o. In other words, λ_t and λ_o are considered known. In such scenarios, Bayes estimation is employed. On the other hand, if the occupancy estimation is applied to an area of interest once, then we should use a classic framework such as maximum likelihood estimation.

3.1 Bayes Estimation

In the Bayes estimation scheme, we assume the Poisson intensity parameters λ_t and λ_o are known. Our objective is to estimate the number of clients inside the target area based on observed data $\underline{\mathbf{P}}$. First, we need to get the posterior distribution of R_t, given $\underline{\mathbf{P}}$,

$$\begin{aligned} \Pr\left(R_t = r_t | \underline{\mathbf{P}} = \underline{\mathbf{p}}\right) &= \int_{\{\underline{\mathbf{u}}: R_t(\underline{\mathbf{u}})=r_t, R_o(\underline{\mathbf{u}})=r_o\}} f_{\underline{\mathbf{U}}|\underline{\mathbf{P}}}\left(\underline{\mathbf{u}}|\underline{\mathbf{p}}\right) d\underline{\mathbf{u}} \\ &= \int_{\{\underline{\mathbf{u}}: R_t(\underline{\mathbf{u}})=r_t, R_o(\underline{\mathbf{u}})=r_o\}} \frac{f_{\underline{\mathbf{P}}|\underline{\mathbf{U}}}\left(\underline{\mathbf{p}}|\underline{\mathbf{u}}\right) f_{\underline{\mathbf{U}}}(\underline{\mathbf{u}})}{f_{\underline{\mathbf{P}}}\left(\underline{\mathbf{p}}\right)} d\underline{\mathbf{u}} \end{aligned} \tag{3.1}$$

where $\underline{\mathbf{U}}$ is the location vector containing the random positions of the wireless clients. The location vector includes lots of information. For example, the size of $\underline{\mathbf{U}}$ is the number of active wireless clients. According to location vector, we can get the number of wireless clients inside or outside the target area. Thus, R_t and R_o are functions of $\underline{\mathbf{U}}$. Because the outside and inside Poisson processes are independent, the distribution of $\underline{\mathbf{U}}$ can be written

as

$$
\begin{aligned}
f_{\underline{\mathbf{U}}}(\underline{\mathbf{u}}) &= \frac{1}{A_{\mathrm{t}}^{R_{\mathrm{t}}(\underline{\mathbf{u}})}} \frac{(\lambda_{\mathrm{t}} A_{\mathrm{t}})^{R_{\mathrm{t}}(\underline{\mathbf{u}})}}{(R_{\mathrm{t}}(\underline{\mathbf{u}}))!} e^{-A_{\mathrm{t}}\lambda_{\mathrm{t}}} \frac{1}{A_{\mathrm{o}}^{R_{\mathrm{o}}(\underline{\mathbf{u}})}} \frac{(\lambda_{\mathrm{o}} A_{\mathrm{o}})^{R_{\mathrm{o}}(\underline{\mathbf{u}})}}{(R_{\mathrm{o}}(\underline{\mathbf{u}}))!} e^{-A_{\mathrm{o}}\lambda_{\mathrm{o}}} \\
&= \frac{\lambda_{\mathrm{t}}^{R_{\mathrm{t}}(\underline{\mathbf{u}})}}{(R_{\mathrm{t}}(\underline{\mathbf{u}}))!} \frac{\lambda_{\mathrm{o}}^{R_{\mathrm{o}}(\underline{\mathbf{u}})}}{(R_{\mathrm{o}}(\underline{\mathbf{u}}))!} e^{-A_{\mathrm{t}}\lambda_{\mathrm{t}} - A_{\mathrm{o}}\lambda_{\mathrm{o}}}.
\end{aligned} \tag{3.2}
$$

For a wireless client j, the distribution of the received power vector $\mathbf{P}_j$ given a specific location $\mathbf{u}_j$ is equal to

$$
\begin{aligned}
f_{\mathbf{P}_j|\mathbf{U}_j}(\mathbf{p}_j|\mathbf{u}_j) &= \prod_{i=1}^{n_{\mathrm{s}}} f_{L_{ij}}(p_{ij} - A - B\log_{10}(d_{ij}) - G_i(\phi_{ij})) \\
&= \frac{1}{\left(2\pi\sigma_{\mathrm{s}}^2\right)^{\frac{n_{\mathrm{s}}}{2}}} \prod_{i=1}^{n_{\mathrm{s}}} e^{-\frac{(p_{ij} - A - B\log_{10}(d_{ij}) - G_i(\phi_{ij}))^2}{2\sigma_{\mathrm{s}}^2}} \\
&= \left(2\pi\sigma_{\mathrm{s}}^2\right)^{-\frac{n_{\mathrm{s}}}{2}} e^{-\frac{\sum_{i=1}^{n_{\mathrm{s}}} (p_{ij} - A - B\log_{10}(d_{ij}) - G_i(\phi_{ij}))^2}{2\sigma_{\mathrm{s}}^2}}.
\end{aligned} \tag{3.3}
$$

The conditional distribution of $\underline{\mathbf{P}}$ given $\underline{\mathbf{U}} = \underline{\mathbf{u}}$, is

$$
f_{\underline{\mathbf{P}}|\underline{\mathbf{U}}}\left(\underline{\mathbf{p}}|\underline{\mathbf{u}}\right) = \prod_{j=1}^{n_{\mathrm{a}}} f_{\mathbf{P}_j|\mathbf{U}_j}(\mathbf{p}_j|\mathbf{u}_j). \tag{3.4}
$$

With the conditional distribution of $\underline{\mathbf{P}}$ given $\underline{\mathbf{U}} = \underline{\mathbf{u}}$ and distribution of $\underline{\mathbf{U}}$, we can compute the marginal distribution of $\underline{\mathbf{P}}$,

$$
\begin{aligned}
f_{\underline{\mathbf{P}}}\left(\underline{\mathbf{p}}\right) &= \int_{\{\underline{\mathbf{u}}: R_{\mathrm{t}}(\underline{\mathbf{u}}) + R_{\mathrm{o}}(\underline{\mathbf{u}}) = n_{\mathrm{a}}\}} f_{\underline{\mathbf{P}}|\underline{\mathbf{U}}}\left(\underline{\mathbf{p}}|\underline{\mathbf{u}}\right) f_{\underline{\mathbf{U}}}(\underline{\mathbf{u}}) d\underline{\mathbf{u}} \\
&= \sum_{(r_{\mathrm{t}}, r_{\mathrm{o}}): r_{\mathrm{t}} + r_{\mathrm{o}} = n_{\mathrm{a}}} \sum_{\{\mathbb{I} \subset [n_{\mathrm{a}}]: |\mathbb{I}| = r_{\mathrm{t}}\}} \frac{\lambda_{\mathrm{t}}^{r_{\mathrm{t}}} \lambda_{\mathrm{o}}^{r_{\mathrm{o}}}}{r_{\mathrm{t}}! r_{\mathrm{o}}!} e^{-A_{\mathrm{t}}\lambda_{\mathrm{t}} - A_{\mathrm{o}}\lambda_{\mathrm{o}}} \\
&\quad \times \prod_{j \in \mathbb{I}} \mathscr{I}_{\mathscr{A}_{\mathrm{t}}}(j) \prod_{j \in \mathbb{I}^{\mathrm{c}}} \mathscr{I}_{\mathscr{A}_{\mathrm{o}}}(j),
\end{aligned}
$$

where the integral components are defined by

$$
\mathscr{I}_{\mathscr{A}_{\mathrm{t}}}(j) = \int_{\mathscr{A}_{\mathrm{t}}} f_{\mathbf{P}_j|\mathbf{U}_j}(\mathbf{p}_j|\mathbf{u}_j) d\mathbf{u}_j \tag{3.5}
$$

$$
\mathscr{I}_{\mathscr{A}_{\mathrm{o}}}(j) = \int_{\mathscr{A}_{\mathrm{o}}} f_{\mathbf{P}_j|\mathbf{U}_j}(\mathbf{p}_j|\mathbf{u}_j) d\mathbf{u}_j. \tag{3.6}
$$

Finally the posterior distribution of R_t, conditional on the gathered data is given as

$$\begin{aligned}&\Pr\left(R_{\mathrm{t}}=r_{\mathrm{t}}|\underline{\mathbf{P}}=\underline{\mathbf{p}}\right)\\&=\sum_{\{\mathbb{I}\subset[n_{\mathrm{a}}]:|\mathbb{I}|=r_{\mathrm{t}}\}}\frac{\lambda_{\mathrm{t}}^{r_{\mathrm{t}}}\lambda_{\mathrm{o}}^{r_{\mathrm{o}}}e^{-A_{\mathrm{t}}\lambda_{\mathrm{t}}-A_{\mathrm{o}}\lambda_{\mathrm{o}}}}{r_{\mathrm{t}}!r_{\mathrm{o}}!f_{\underline{\mathbf{P}}}(\underline{\mathbf{p}})}\prod_{j\in\mathbb{I}}\mathscr{I}_{\mathscr{A}_{\mathrm{t}}}(j)\prod_{j\in\mathbb{I}^{\mathrm{c}}}\mathscr{I}_{\mathscr{A}_{\mathrm{o}}}(j).\end{aligned}$$

Computing this conditional distribution of R_t given $\underline{\mathbf{P}}$ may appear difficult as it needs to take sums over subsets of $\{1,\ldots,n_{\mathrm{a}}\}$. However, by using generating functions, the posterior distribution can be calculated more efficiently [25].

Thus, the mean of the posterior distribution of R_t condition upon $\underline{\mathbf{P}}$ is the Bayes estimator,

$$\hat{R}_{\mathrm{t}}\left(\underline{\mathbf{p}}\right)=\mathrm{E}\left[R_{\mathrm{t}}|\underline{\mathbf{P}}=\underline{\mathbf{p}}\right]=\sum_{r_{\mathrm{t}}=0}^{n_{\mathrm{a}}}r_{\mathrm{t}}\Pr\left(R_{\mathrm{t}}=r_{\mathrm{t}}|\underline{\mathbf{P}}=\underline{\mathbf{p}}\right). \tag{3.7}$$

We adopt Bayesian mean squared error to evaluate the performance of the estimator, which is given below.

$$\mathrm{BMSE}\left[\hat{R}_{\mathrm{t}}\right]=\mathrm{E}\left[\left(\hat{R}_{\mathrm{t}}\left(\underline{\mathbf{P}}\right)-R_{\mathrm{t}}\right)^2\right]. \tag{3.8}$$

This BMSE can be approximated by taking the average over samples numerically.

$$\mathrm{BMSE}\left[\hat{R}_{\mathrm{t}}\right]\approx\frac{1}{M}\sum_{m=1}^{M}\left(\hat{R}_{\mathrm{t}}^{(m)}\left(\underline{\mathbf{P}}^{(m)}\right)-R_{\mathrm{t}}^{(m)}\right)^2. \tag{3.9}$$

3.2 Maximum likelihood estimation

In this section, we assume the Poisson intensity parameters λ_{t} and λ_{o} are unavailable. In this case we will employ a classical approach and adopt maximum-likelihood estimation [26]. The distribution of $\underline{\mathbf{U}}$ can be written as

$$f_{\underline{\mathbf{U}}}\left(\underline{\mathbf{u}};\lambda_{\mathrm{t}},\lambda_{\mathrm{o}}\right)=\frac{\lambda_{\mathrm{t}}^{R_{\mathrm{t}}(\underline{\mathbf{u}})}}{(R_{\mathrm{t}}(\underline{\mathbf{u}}))!}\frac{\lambda_{\mathrm{o}}^{R_{\mathrm{o}}(\underline{\mathbf{u}})}}{(R_{\mathrm{o}}(\underline{\mathbf{u}}))!}e^{-A_{\mathrm{t}}\lambda_{\mathrm{t}}-A_{\mathrm{o}}\lambda_{\mathrm{o}}}. \tag{3.10}$$

The likelihood function is a function with two parameters, λ_t and λ_o

$$\begin{aligned}\mathscr{L}\left(\lambda_t,\lambda_o;\underline{\mathbf{p}},\underline{\mathbf{u}}\right) &= f_{\underline{\mathbf{P}},\underline{\mathbf{U}}}\left(\underline{\mathbf{p}},\underline{\mathbf{u}};\lambda_t,\lambda_o\right)\\ &= f_{\underline{\mathbf{P}}|\underline{\mathbf{U}}}\left(\underline{\mathbf{p}}|\underline{\mathbf{u}}\right) f_{\underline{\mathbf{U}}}\left(\underline{\mathbf{u}};\lambda_t,\lambda_o\right).\end{aligned} \tag{3.11}$$

By computing the integral over $\underline{\mathbf{U}}$, we can get the marginal likelihood function

$$\begin{aligned}&\mathscr{L}\left(\lambda_t,\lambda_o;\underline{\mathbf{p}}\right) = \int_{\{\underline{\mathbf{u}}:R_t(\underline{\mathbf{u}})+R_o(\underline{\mathbf{u}})=n_a\}} f_{\underline{\mathbf{P}}|\underline{\mathbf{U}}}\left(\underline{\mathbf{p}}|\underline{\mathbf{u}}\right) f_{\underline{\mathbf{U}}}\left(\underline{\mathbf{u}};\lambda_t,\lambda_o\right) d\underline{\mathbf{u}}\\ &= e^{-A_t\lambda_t - A_o\lambda_o} \sum_{(r_t,r_o):r_t+r_o=n_a} \frac{\lambda_t^{r_t}\lambda_o^{r_o}}{r_t!r_o!} \sum_{\{\mathbb{I}\subset[n_a]:|\mathbb{I}|=r_t\}} \prod_{j\in\mathbb{I}} \mathscr{I}_{\mathscr{A}_t}(j) \prod_{j\in\mathbb{I}^c} \mathscr{I}_{\mathscr{A}_o}(j).\end{aligned} \tag{3.12}$$

This is a two-dimensional optimization, but we can simplify it to a one-dimensional optimization problem by following property,

$$\max_{\lambda_t,\lambda_o} \mathscr{L}\left(\lambda_t,\lambda_o;\underline{\mathbf{p}}\right) = \max_{\alpha} \mathscr{L}\left(\frac{n_a}{A_t}\alpha, \frac{n_a}{A_o}(1-\alpha);\underline{\mathbf{p}}\right) \tag{3.13}$$

where α within the interval $[0,1]$. Therefore, we rewrite the likelihood function in terms of α

$$\begin{aligned}&\mathscr{L}\left(\frac{n_a}{A_t}\alpha, \frac{n_a}{A_o}(1-\alpha);\underline{\mathbf{p}}\right)\\ &= \sum_{(r_t,r_o):r_t+r_o=n_a} \frac{e^{-n_a}n_a^{n_a}}{r_t!r_o!} \left(\frac{\alpha}{A_t}\right)^{r_t} \left(\frac{1-\alpha}{A_o}\right)^{r_o} \sum_{\{\mathbb{I}\subset[n_a]:|\mathbb{I}|=r_t\}} \prod_{j\in\mathbb{I}} \mathscr{I}_{\mathscr{A}_t}(j) \prod_{j\in\mathbb{I}^c} \mathscr{I}_{\mathscr{A}_o}(j).\end{aligned} \tag{3.14}$$

Now, we can use numerical methods to get the values of λ_t and λ_o which maximize the likelihood function. Once λ_t and λ_o are obtained, the maximum likelihood estimator can be calculated as

$$\begin{aligned}\hat{R}_t\left(\underline{\mathbf{p}}\right) &= \mathrm{E}_{\hat{\lambda}_t,\hat{\lambda}_o}\left[R_t|\underline{\mathbf{P}}=\underline{\mathbf{p}}\right]\\ &= \sum_{r_t=0}^{n_a} r_t \Pr\left(R_t=r_t|\underline{\mathbf{P}}=\underline{\mathbf{p}};\hat{\lambda}_t,\hat{\lambda}_o\right).\end{aligned} \tag{3.15}$$

We adopt the mean squared error to evaluate the performance of our estimator,

$$\mathrm{MSE}\left[\hat{R}_t\right] = \mathrm{E}\left[\left(\hat{R}_t\left(\underline{\mathbf{P}}\right)-R_t\right)^2\right]. \tag{3.16}$$

This mean squared error can be approximated by taking the average over samples numerically,

$$\mathrm{MSE}\left[\hat{R}_{\mathrm{t}}\right] \approx \frac{1}{M}\sum_{m=1}^{M}\left(\hat{R}_{\mathrm{t}}^{(m)}\left(\underline{\mathbf{P}}^{(m)}\right) - R_{\mathrm{t}}^{(m)}\right)^2. \tag{3.17}$$

4 NUMERICAL SIMULATION SETUP AND RESULTS

In this section, we introduce our simulation setup, including the directional antenna model, the parameters of the channel and how we generate RSSI samples. The simulation results will be shown after that. The simulation code is written in Python. In the simulation framework, the set up consists of four monitoring devices placed at the corners of the area of interest. All antennas attached to monitoring devices are pointing towards the center of the area of interest. The target area is considered to be a square of dimension 6 m × 6 m inscribed in a larger square of dimension 10 m×10 m. The two square areas share a same center point. Again, we use A_t to denote the target area, while A_o denotes its complement. We call the inside region the target area, and we refer to its complement as the outside region in the following text.

4.1 Antenna Characteristic

To analyze the effect of radiation characteristics of the sensing antennas on the estimation, isotropic antennas and directional antennas are considered. The antenna gain of isotropic antennas are zero in all directions. For the directional antennas, we adopt 3GPP antenna model in [27]. The directional antenna gains obey the following formula,

$$G_i(\phi_{ij}) = -\min\left\{12\left(\frac{\phi_{ij}-\theta_i}{\theta_{3\text{dB}}}\right)^2, G_{\text{floor}}\right\} - G_{\text{avg}}$$

where θ_i is pointing direction of the antenna which is attached to monitoring device i. Parameter $\theta_{3\text{dB}}$ is the 3 dB beam-width of the radiation pattern. G_{floor} is a nominal at-

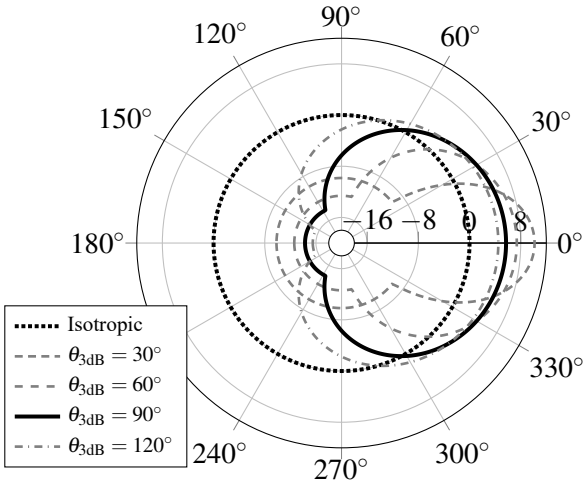

Figure 4.1: This graph depicts normalized antenna radiation patterns. The pointing direction is set to 0° and $G_{\text{floor}} = 20$ dB.

tenuation floor. $G_{average}$ is a normalization factor, which equal to the average gain over $\in (-180°, 180°]$,

$$10\log_{10}\left(\int_{-180}^{180}\frac{10^{-\frac{1}{10}\min\left\{12\left(\frac{\phi_{ij}-\theta_i}{\theta_{3\text{dB}}}\right)^2, G_{\text{floor}}\right\}}}{360}d\phi_{ij}\right).$$

The antenna radiation pattern for various 3 dB beam-widths is shown in Fig. 4.1.

4.2 Channel Characteristic

As mentioned in Chapter 2.1, the channel model we adopt is the log-normal path loss model. The received signal power can be expressed as

$$P[\text{dBm}] = A + B\log_{10}(d) + L + G(\phi). \tag{4.1}$$

In this equation, the physical parameters are based on regulation issued by the Federal Communications Commission (FCC) and on the profiles of typical wireless environments.

According to the Friis transmission equation [28], we have

$$A = P_{\mathrm{t}} + 20\log_{10}\left(\frac{3\times 10^{8}}{f_{\mathrm{carrier}}}\right) - 20\log_{10}(4\pi)$$

where P_t is the mobile devices transmission power, which is set to 20 dBm. The frequency $f_{carrier}$ is that of the Wi-Fi signal wave, 2.462 GHz [29]. Accordingly, A is equal to -20.27 dBm. We set the path-loss parameter B to -20 dBm, which is the coefficient associated with free-space. The logarithmic σ_s, which represents variation in shadow fading, is set to 2.0 dBm.

4.3 Generating Data Set

As mentioned above, the inference task is based on the received power matrix, which is collected by the monitoring devices. In the simulation, we generate the sample data according to the antenna gain model and the channel model discussed above. The parameter values we use to create the data set are summarized in Table 4.1. We generate the numerical data set as follow. We denote the location of the four monitoring devices as $\{\mathbf{s}_i\}$ $i \in 1,2,3,4$. First, we set a certain value λ, which represents the aggregate Poisson rate across the two monitored regions (inside region and outside region) equal to 32. The split-

Table 4.1: System parameters used during simulations.

Physical Parameters	**Values**
Nominal Power	$A = -20.27$ dBm
Free-Space Loss parameter	$B = -20$ dBm
Logarithmic Standard Deviation	$\sigma_{\mathrm{s}} = 2.0$ dBm
3 dB Beam-width (directional)	$\theta_{3\mathrm{dB}} = 90^{\circ}$
Antenna Floor	$G_{\mathrm{floor}} = 20$ dB

ting parameter between two regions is α. Thus,

$$\lambda_{\mathrm{t}} = \alpha \frac{\lambda}{A_{\mathrm{t}}} \qquad\qquad \lambda_{\mathrm{o}} = (1-\alpha)\frac{\lambda}{A_{\mathrm{o}}}$$

where λ_t is the Poisson rate of inside region and λ_o is the Poisson rate of outside region. Once λ_t and λ_o are determined, r_t the number of devices inside and r_o the number of devices outside are established using Poisson trials,

$$R_{\mathrm{t}} \sim \frac{(A_{\mathrm{t}}\lambda_{\mathrm{t}})^k}{k!} e^{-A_{\mathrm{t}}\lambda_{\mathrm{t}}} \qquad\qquad R_{\mathrm{o}} \sim \frac{(A_{\mathrm{o}}\lambda_{\mathrm{o}})^k}{k!} e^{-A_{\mathrm{o}}\lambda_{\mathrm{o}}}.$$

Each of $R_t = r_t$ devices inside the target area is independently assigned a location according to a uniform distribution. Likewise, each of $R_{\mathrm{o}} = r_{\mathrm{o}}$ devices outside is independently assigned a location according to another uniform distribution. Therefore, we obtain the location vector $\underline{\mathbf{U}} = \underline{\mathbf{u}}$ of the wireless clients. For each of the wireless clients, a collection of four received signal strength corresponding to the four monitoring devices is computed according to (4.1). The shadow fading component L is generated following a log-normal distribution whose standard deviation $\sigma_s = 2.0$ dBm. Finally, we get the sequence of power vectors $\underline{\mathbf{p}} = (\mathbf{p}_1, \ldots, \mathbf{p}_{n_{\mathrm{a}}})$, where vector $\mathbf{p}_j$ corresponding to wireless client j contains four power strength received by four monitoring devices respectively.

4.4 Performance Analysis

The proposed estimators act on observation vector $\mathbf{p}$

4.4.1 Bayes Estimation

We first consider the performance of the Bayes estimation framework introduced in Section 3.1. As is discussed in the previous section, the Poisson rate of the combined two

regions λ, the Poisson rate of inside region λ_t and the Poisson rate of outside region λ_o have the following relation along with the splitting parameter α,

$$\lambda_{\mathrm{t}} = \alpha \frac{\lambda}{A_{\mathrm{t}}} \qquad\qquad \lambda_{\mathrm{o}} = (1-\alpha)\frac{\lambda}{A_{\mathrm{o}}}.$$

In the simulation results, the area of inside region A_t is equal to 36, and the area of outside region A_o is equal to 64. We can plot performance results as a function of the splitting coefficient α. The vertical axis represents the BMSE of Bayes estimator. The black curve in Fig. 4.2 shows the BMSE when the Bayes estimator operates on data collected using isotropic antennas. The red curve in Fig. 4.2 corresponds to four directional antennas located at the four corners of the target area and pointing directly to the center. These antennas have a 3 dB beam-width of $\theta_{3\mathrm{dB}} = 90^\circ$ and a nominal attenuation floor of $G_{\mathrm{floor}} = 20$ dB. Every point is obtained by averaging over fifty thousand trials. According to Fig. 4.2, systems with directional antennas perform better than systems with isotropic antennas.

To further compare the performances, we introduce confidence intervals. A confidence level refers to the percentage of all possible samples that can be expected to include the true population parameter [30]. Suppose we use the same sampling method to select different samples and to compute a different interval estimate for each sample. Some interval estimates would include the true population parameter and some may not. A 95% confidence level means that 95% of the intervals would include the true parameter. Generally, the confidence interval is computed as below. Select a confidence level which describes

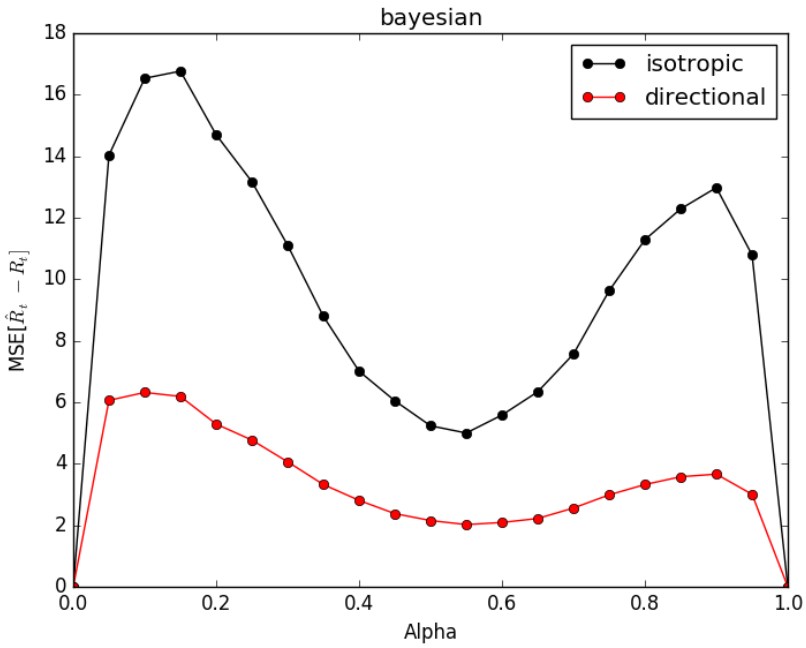

Figure 4.2: This graph shows Bayesian mean squared error as functions of splitting parameter under scheme of 3.1. Black line correspond to performance of system equipped with isotropic antennas, whereas red line correspond to the performance of systems with directional antennas.

the uncertainty of a sampling method. Compute α,

$$\alpha = 1 - (\text{confidence level}/100).$$

Find the critical probability p^*

$$p^* = 1 - \alpha/2.$$

Express the critical value as a t-statistic by using degree of freedom and critical probability, where degree of freedom equals to

$$df = N - 1$$

and N is the sample size. The standard error SE is given as

$$SE = \frac{\sigma}{\sqrt{N}}$$

where σ is the standard deviation of the sample. The magin of error is the product of critical value t^* and SE. The confidence interval is expressed as

$$\text{Confidence interval} = \mu \pm \text{Margin of error}$$

where μ is the mean of the sample. In this simulation, we analyze the absolute difference between the real number of active devices inside r_t and the estimator result $\hat{r}_t$. The confidence intervals of $|r_t - \hat{r}_t|$ corresponding to isotropic antennas and directional antennas are summarized in Table 4.2. The result is based on fifty thousand samples. To make the

Table 4.2: Confidence interval of $|r_t - \hat{r}_t|$ for simulation Bayes scheme

Antenna type	**Confidence interval**	**Confidence level**
Directional	1.412411 ± 0.002166	95%
Isotropic	2.454623 ± 0.003450	95%

result more straightforward, we use Gaussian kernel density estimation to plot the approx-

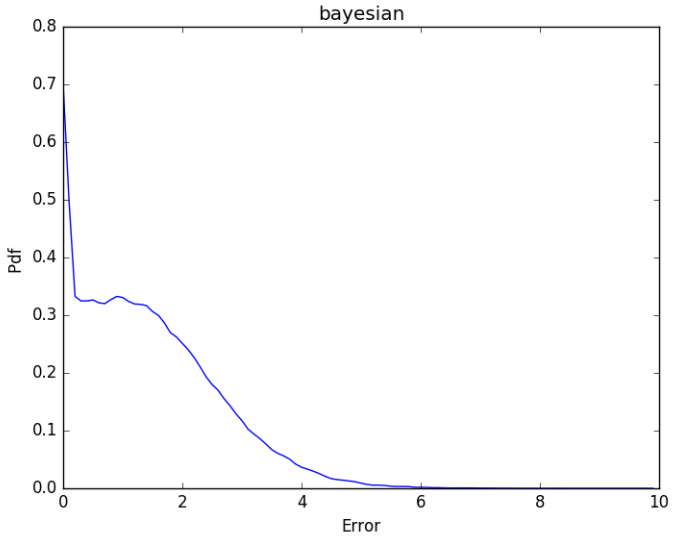

Figure 4.3: This graph shows the approximation probability density function of $|r_t - \hat{r}_t|$ corresponding to system equipped with directional antennas under the scheme of Section 3.1.

imation of the probability density function of $|r_t - \hat{r}_t|$. The horizontal axis represents value for $|r_t - \hat{r}_t|$. Comparing the PDF curves in Fig. 4.3 and Fig. 4.4, the distribution of the error occurs in system with directional antennas appears closer to zero. This result, along with fact that the BMSE of directional systems is smaller, shows that systems with directional antennas perform better. This performance improvement results from the directional antennas being more discriminating than the isotropic antennas.

4.4.2 Maximum Likelihood Estimation

In this section, we look into the maximum likelihood estimation framework mentioned in Section 3.2. We use the average mean squared error to evaluate the performance of our estimator. As before, the total Poisson rates is set to be 32 and the curves are functions of splitting coefficient α. The black curve in Fig. 4.5 shows the MSE when the

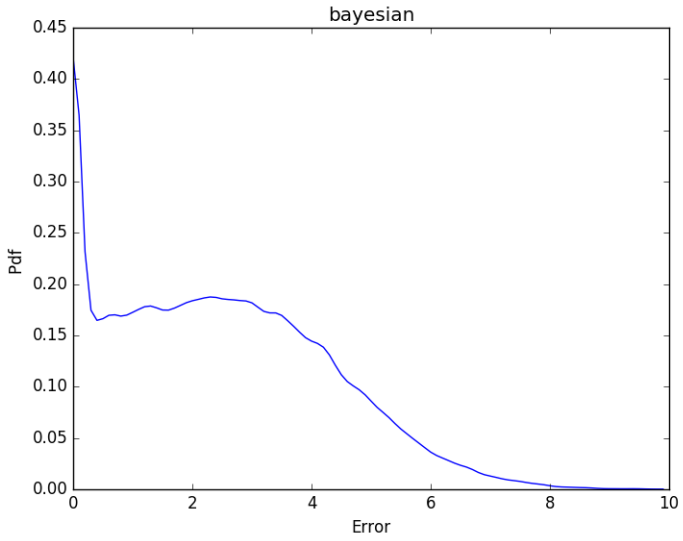

Figure 4.4: This graph shows the approximation probability density function of $|r_t - \hat{r}_t|$ corresponding to system equipped with isotropic antennas under scheme of 3.1.

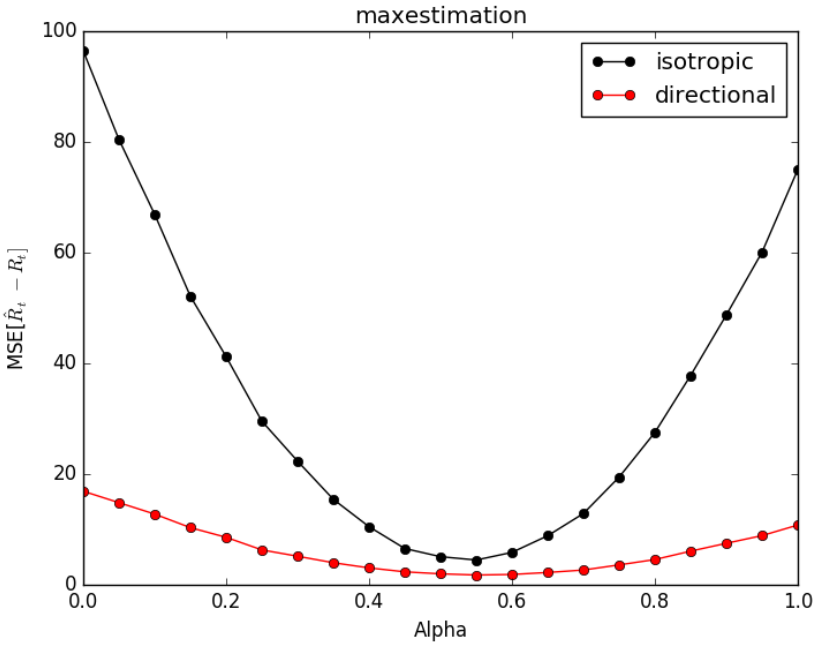

Figure 4.5: This figure shows mean squared error as functions of splitting parameter under scheme of Section 3.2. Black line correspond to performance of system equipped with isotropic antennas, whereas red line correspond to the performance of systems with directional antennas.

maximum likelihood estimator operates on data collected using isotropic antennas. The red curve in Fig. 4.5 corresponds to the scenario where the estimator operates on data collected by directional antennas. The four directional antennas are located at the four corners of the target area, and they are pointing directly towards the center. These antennas have a 3 dB beam-width of $\theta_{3\text{dB}} = 90^\circ$ and a nominal attenuation floor of $G_{\text{floor}} = 20$ dB. Every point is obtained by averaging over fifty thousand trials. The MSE is smaller for systems using directional antennas.

The confidence interval of the absolute error $|r_t - \hat{r}_t|$ corresponding to the isotropic antennas and the directional antennas are summarized in Table 4.3. Compared the PDF

Table 4.3: Confidence interval of $|r_t - \hat{r}_t|$ for simulation corresponding to the Maximum likelihood scheme.

Antenna type	**Confidence interval**	**Confidence level**
Directional	2.080484 ± 0.002809	95%
Isotropic	4.972427 ± 0.006020	95%

curves in Fig. 4.6 and Fig. 4.7, we see that the distribution of the error for systems with directional antennas appears closer to zero. This result, along with the fact that the MSE for the directional systems is smaller, shows that directional antennas outperform isotropic antennas within this context. Again, these results indicate that the information obtained from the directional antennas is more discriminating than the isotropic antennas.

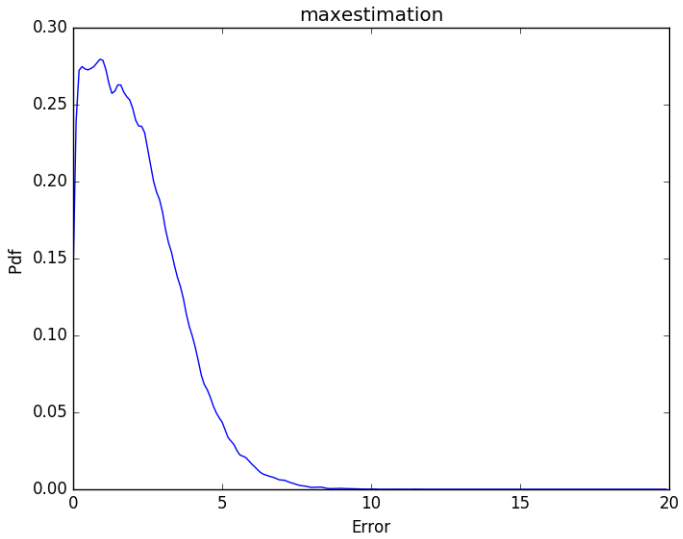

Figure 4.6: This graph shows the approximation probability density function of $|r_t - \hat{r}_t|$ corresponding to system equipped with directional antennas under scheme of 3.2.

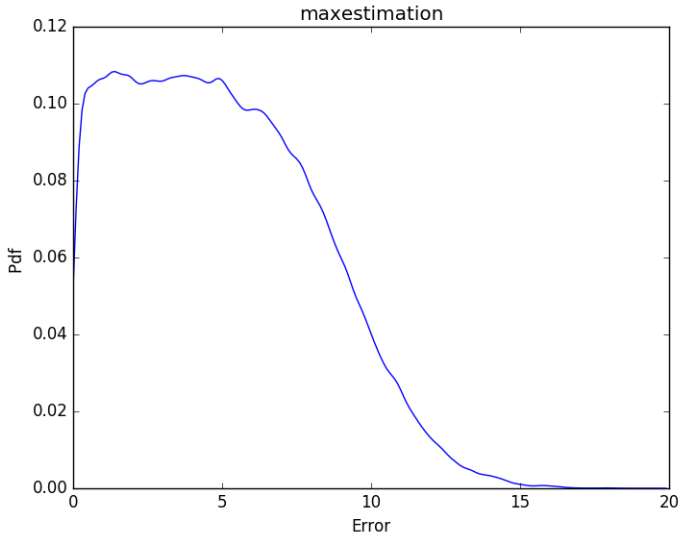

Figure 4.7: This graph shows the approximation probability density function of $|r_t - \hat{r}_t|$ corresponding to system equipped with isotropic antennas under scheme of 3.2.

5 EXPERIMENTAL IMPLEMENTATION

To complement the numerical findings based on our theoretical framework. We take an experimental implementation to assess two schemes proposed in this work. The RSSI signal strength data set is collected during experiment. This information is also used to provide statistical evidence for the wireless channel model adopted throughout. This model is used to determine the characteristics of the environment. The system is designed to work on the 2.4 GHz ISM radio band which is used by Wi-Fi technology. In this experiment, all wireless clients are connected to a wireless access point. This chapter details the way the experiments are designed, and explains the analysis of the gathered information.

5.1 Monitoring Devices

Every sensing device takes the form of a Next Unit of Computing (NUC) by Intel™, and runs on Ubuntu 14.04 operation system. Wireless monitoring is enabled through an Alfa™ `AWUS036NHA` wireless interface with a detachable antenna. The Atheros™ chipset is able to listen to transmission packets on a channel if turned on monitoring mode. The sub-miniature version A antenna connectors are used to attach either isotropic antennas or directional antennas. Each monitoring device is attached with one directional antenna and one isotropic antenna. Wooden sticks are also used to fix the two antennas attached to one monitoring devices at different heights in order to reduce the interference influence between two antennas. The radiation pattern of directional antenna is shown in Fig. 5.1. A

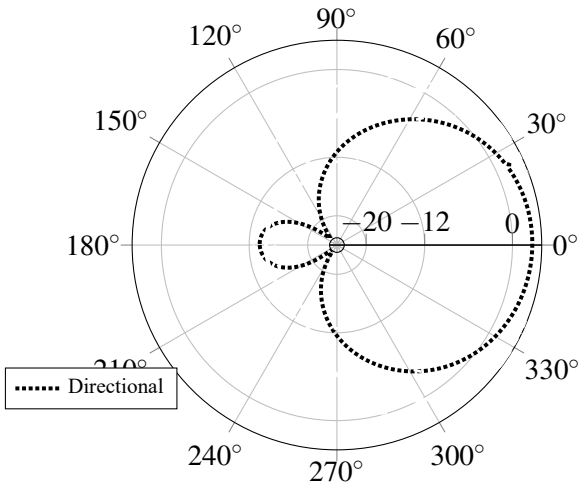

Figure 5.1: This graph depicts directional antenna radiation patterns

sniffing software build on the *pcap* application programming interface captures and filters wireless packets. For filtering, we employ a hash table for removing the duplicates in the detected MAC addresses. The software creates a local database to store MAC address and RSSI extracted from the wireless packets it receives. Finally the local database is sent to a central server for processing. The monitoring device we used during experiment is shown in Fig. 5.2.

5.2 Wireless client

In our experiment, the wireless clients are Android™ smartphones. All the wireless clients connect to a same local access point and send packets periodically which makes them detected by sniffing software. For the purpose of evaluate the performance of estimator, not only we need RSSI values, but we also need the ground truth (i.e. the location of the wireless clients). Thus we employ a custom app, which logs GPS coordinates and

Figure 5.2: This graph shows the monitoring device we use.

time. While conducting experiment, wireless clients periodically transmit the GPS information collected by app to a central server. MAC addresses and time stamps are then used to match locations to power vectors at the center server, yielding a data set for performance evaluation.

5.3 Experimental Samples

The experimental samples are divided into two categories, one is for monitoring devices with isotropic antennas, the other is for monitoring devices with directional antennas. Each category contains about 400 power and location vectors. Each power vector is in this form, $\underline{\mathbf{p}} = (\mathbf{p}_1, \ldots, \mathbf{p}_4)$, where $\mathbf{p}_i$ is the power received by i monitoring device. Since there are four monitoring devices, we have almost 3200 distinct points of RSSI. For conduct

experimental trail as following. Firstly, generate the number of active clients inside t and number of active clients outside o according to two Poisson distribution with parameter λ_t and $\lambda_{[o]}$ respectively.

$$\lambda_{\mathrm{t}} = \alpha\frac{\lambda}{A_{\mathrm{t}}} \qquad\qquad \lambda_{\mathrm{o}} = (1-\alpha)\frac{\lambda}{A_{\mathrm{o}}}.$$

Then r_t entries are selected uniformly from clients in A_t, and r_o entries are selected uniformly from clients in A_o. The two collections of entries are combined into a single vector $\underline{\mathbf{p}}$, which is the input to the estimator. At last, the estimates are evaluated through the ground truth.

5.4 Channel Parameters

Channel parameters A and B can vary depending on the wireless environment. This experiment is conducted on widely open parking lot. Fig. offers a satellite image view of the experiment site. The parameters are obtained by using least squares method mentioned in 2.1. The parameters for the isotropic systems are $A = -41.68, B = -16.07$ and $\sigma_s = 7.91dBm$. Similarly, the parameters for the systems with directional antennas are $A = -34.72, B = -17.11$ and $\sigma_s = 8.31dBm$

5.5 Experiment Results

5.5.1 Performance of Bayes Estimation

Experimental curves under Bayes estimation scheme is shown in Fig. 5.4. The horizontal axis is the splitting parameter α. The vertical axis is the BMSE. Each point is av-

Figure 5.3: This figure highlights the site used for the experiments and marks locations of experiment data.

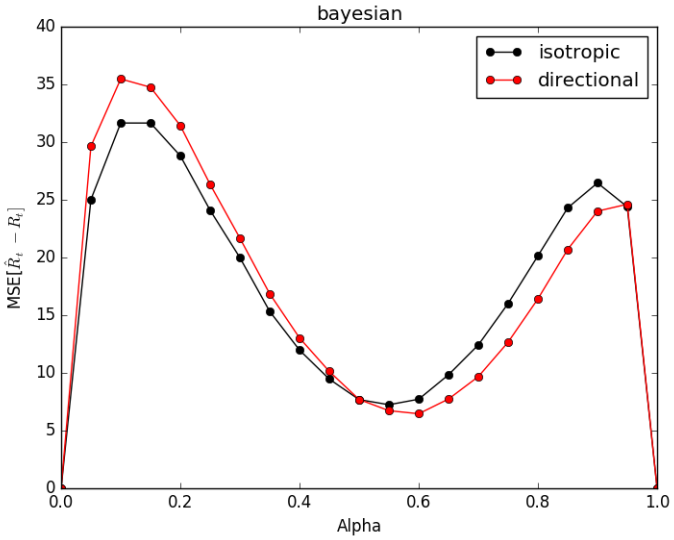

Figure 5.4: This figure depicts the experimental Bayesian mean squared error as function of Poisson splitting coefficient α. Red line represents systems with directional antennas, whereas black line represent system with isotropic antennas.

eraging over 10000 trails. The confidence intervals of $|r_t - \hat{r}_t|$ corresponding to isotropic antennas and directional antennas are summarized in Table 5.1. The approximation prob-

Table 5.1: Confidence interval of $|r_t - \hat{r}_t|$ for experimental Bayes scheme

Antenna type	**Confidence interval**	**Confidence level**
Directional	3.317535 ± 0.010430	95%
Isotropic	3.331094 ± 0.010274	95%

ability density functions corresponding to systems with directional antennas and isotropic antennas are shown in Fig. 5.5 and Fig. 5.6. In this case using directional antennas does not bring an obvious benefit. The BMSE of systems with directional antennas and that with isotropic antennas are very close. As well as the confidence intervals and the absolute error distribution. This phenomena maybe caused by the inaccuracy of GPS information. Some small location errors may bring large errors, especially for the case when using directional

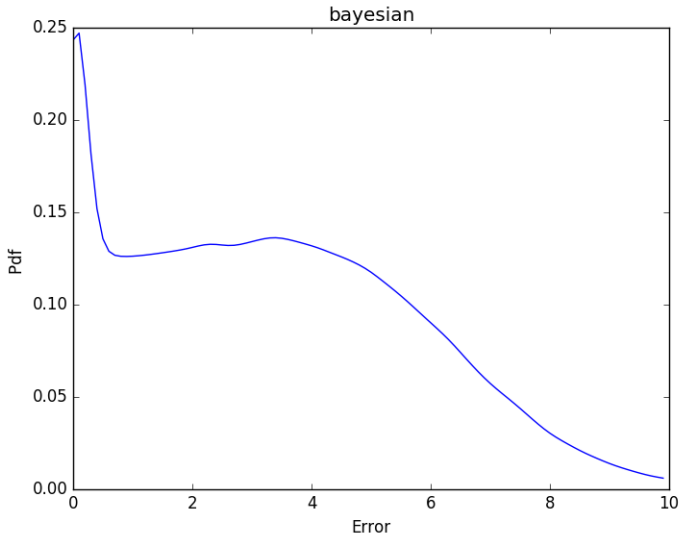

Figure 5.5: This graph shows the approximation probability density function of $|r_t - \hat{r}_t|$ corresponding to system equipped with directional antennas under scheme of 3.1.

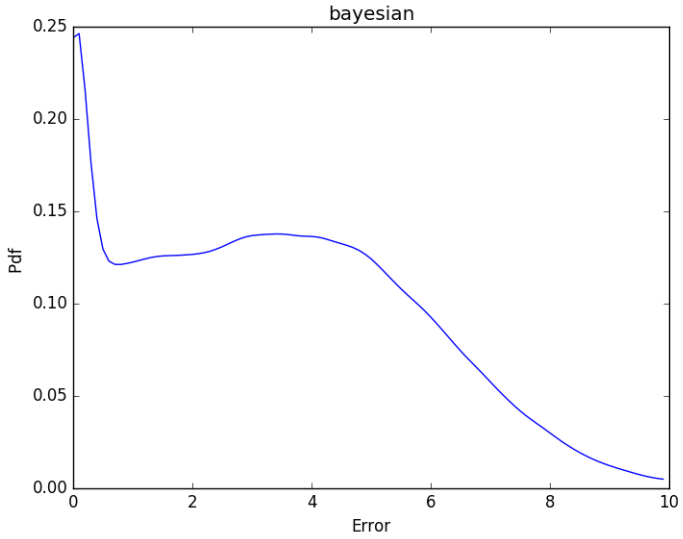

Figure 5.6: This graph shows the approximation probability density function of $|r_t - \hat{r}_t|$ corresponding to system equipped with isotropic antennas under scheme of 3.1.

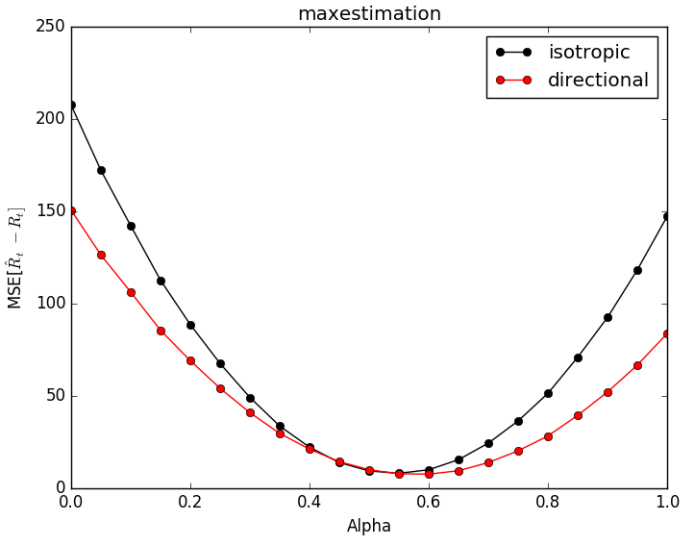

Figure 5.7: This figure depicts the experimental Bayesian mean squared error as function of Poisson splitting coefficient α. Red line represents systems with directional antennas, whereas black line represent system with isotropic antennas.

antennas.

5.5.2 Performance of Maximum Estimation

Experimental curves under Bayes estimation scheme is shown in Fig. 5.7. The horizontal axis is the splitting parameter α. The vertical axis is the BMSE. Each point is averaging over 10000 trails. The confidence intervals of $|r_t - \hat{r}_t|$ corresponding to isotropic antennas and directional antennas are summarized in Table 5.2. The approximation prob-

Table 5.2: Confidence interval of $|r_t - \hat{r}_t|$ for experimental Maximum estimation scheme

Antenna type	**Confidence interval**	**Confidence level**
Directional	5.881027 ± 0.016484	95%
Isotropic	7.144900 ± 0.019182	95%

ability density functions corresponding to systems with directional antennas and isotropic antennas are shown in Fig. 5.8 and Fig. 5.9. In this case, systems with directional antennas

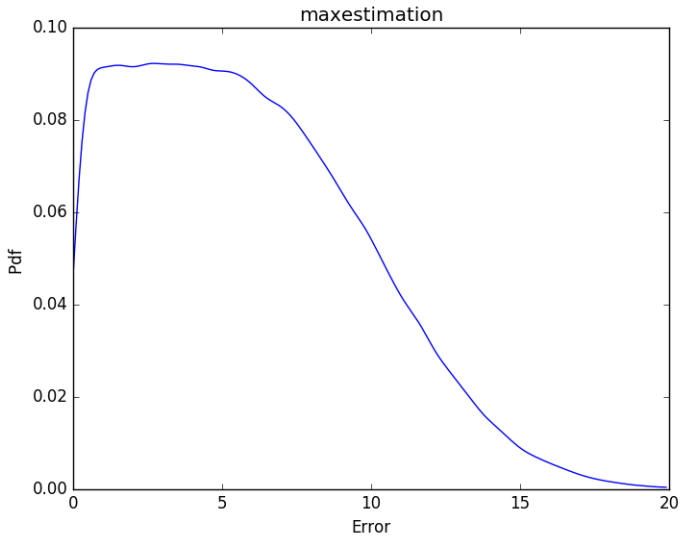

Figure 5.8: This graph shows the approximation probability density function of $|r_t - \hat{r}_t|$ corresponding to system equipped with directional antennas under scheme of 3.2.

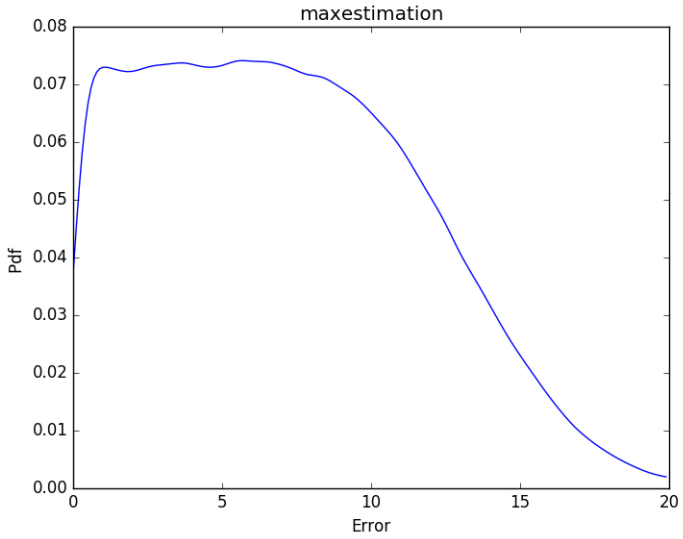

Figure 5.9: This graph shows the approximation probability density function of $|r_t - \hat{r}_t|$ corresponding to system equipped with isotropic antennas under scheme of 3.2.

better, which means systems equipped with direcional antennas are more discrimination.

6 CONCLUSION

In this thesis, we report two algorithms corresponding to different application scenarios for occupancy estimation using Wi-Fi monitoring. We serves NUC with sensing antenna as monitoring device. We test the estimators performance with isotropic and directional antennas through numerical simulation and experimental implementation. Our result indicates that it is possible to accurately estimate the number of active agents within a prescribed area by deploying sensing devices about the area of interest, and that performance is generally enhanced by the careful shaping of antenna radiation patterns. Performance of a monitoring system can then be enhanced by employing a configuration that strongly discriminates between wireless agents that are located within or outside the target area. In general, a more discriminating configuration yields considerable improvements over a generic setup with isotropic antennas.

This work can be extended for future research. This includes tracking occupancy over time. It also includes estimate the density of person using non-uniform distributions. It is also interesting to use reconfigurable antennas to acquire very discriminating information about active devices for the wireless inference. Finally, the goal would be reality implementation such as indoor monitoring where multipath fading exists and tracking the movement of any particular active device. This information can be used to dynamically adapting Wi-Fi access point to network traffic conditions.

REFERENCES

[1] T. A. Nguyen and M. Aiello, "Energy intelligent buildings based on user activity: A survey," *Energy and Buildings*, vol. 56, pp. 244 – 257, 2013.

[2] B. Balaji, J. Xu, A. Nwokafor, R. Gupta, and Y. Agarwal, "Sentinel: Occupancy based hvac actuation using existing wifi infrastructure within commercial buildings," in *Proceedings of the 11th ACM Conference on Embedded Networked Sensor Systems*, SenSys '13, (New York, NY, USA), pp. 17:1–17:14, ACM, 2013.

[3] D. Valerio, A. D'Alconzo, F. Ricciato, and W. Wiedermann, "Exploiting cellular networks for road traffic estimation: A survey and a research roadmap," in *Vehicular Technology Conference, 2009. VTC Spring 2009. IEEE 69th*, pp. 1–5, April 2009.

[4] Cisco Systems, Inc., *Visual Networking Index: Global Mobile Data Traffic Forecast Update*, 2016.

[5] C. Xu, B. Firner, R. S. Moore, Y. Zhang, W. Trappe, R. Howard, F. Zhang, and N. An, "Scpl: Indoor device-free multi-subject counting and localization using radio signal strength," in *Proceedings of the 12th International Conference on Information Processing in Sensor Networks*, IPSN '13, (New York, NY, USA), pp. 79–90, ACM, 2013.

[6] M. Seifeldin, A. Saeed, A. E. Kosba, A. El-Keyi, and M. Youssef, "Nuzzer: A large-scale device-free passive localization system for wireless environments," *IEEE Transactions on Mobile Computing*, vol. 12, pp. 1321–1334, July 2013.

[7] eMarketer, Inc., *Worldwide Internet and Mobile Users: eMarketer's Updated Estimates for 2015*, 2015.

[8] comScore, *comScore Reports December 2015 U.S. Smartphone Subscriber Market Share*, 2015.

[9] T. S. Rappaport *et al.*, *Wireless communications: principles and practice*, vol. 2. Prentice Hall PTR New Jersey, 1996.

[10] H. L. Bertoni, *Radio propagation for modern wireless systems*. Pearson Education, 1999.

[11] G. L. Stüber, *Principles of mobile communication*. Springer Science & Business Media, 2011.

[12] Z. Ma and A. B. Chan, "Crossing the line: Crowd counting by integer programming with local features," in *The IEEE Conference on Computer Vision and Pattern Recognition (CVPR)*, June 2013.

[13] Y. Taniguchi, M. Mizushima, G. Hasegawa, H. Nakano, and M. Matsuoka, "Counting pedestrians passing through a line in crowded scenes by extracting optical flows," *International Information Institute (Tokyo).Information*, vol. 19, pp. 303–316, 01 2016.

Copyright - Copyright International Information Institute Jan 2016; Document feature - Illustrations; Equations; Tables; Graphs; ; Last updated - 2016-07-30.

[14] M. Li, Z. Zhang, K. Huang, and T. Tan, "Estimating the number of people in crowded scenes by mid based foreground segmentation and head-shoulder detection," in *Pattern Recognition, 2008. ICPR 2008. 19th International Conference on*, pp. 1–4, IEEE, 2008.

[15] V. Garg and N. Bansal, "Smart occupancy sensors to reduce energy consumption," *Energy and Buildings*, vol. 32, no. 1, pp. 81 – 87, 2000.

[16] O. Shih and A. Rowe, "Occupancy estimation using ultrasonic chirps," in *Proceedings of the ACM/IEEE Sixth International Conference on Cyber-Physical Systems*, ICCPS '15, (New York, NY, USA), pp. 149–158, ACM, 2015.

[17] Nishide, R., and H. Takada, "Exploring efficient methods to extract pedestrian flows on a mobile adhoc network," *The 6th International Conference on Mobile Ubiquitous Computing, Systems, Services and Technologies*, 2012.

[18] Depatla, Saandeep, Arjun Muralidharan, and Yasamin Mostofi, "Occupancy estimation using only wifi power measurements," *IEEE Journal on Selected Areas in Communications*, vol. 33, pp. 1381–1393, 05 2015.

[19] N. Abedi, A. Bhaskar, and E. Chung, "Bluetooth and wi-fi mac address based crowd data collection and monitoring : benefits, challenges and enhancement," in *36th Aus-*

tralasian Transport Research Forum (ATRF), (Queensland University of Technology, Brisbane, QLD), October 2013.

[20] W. Xi, J. Zhao, X. Y. Li, K. Zhao, S. Tang, X. Liu, and Z. Jiang, "Electronic frog eye: Counting crowd using wifi," in *IEEE INFOCOM 2014 - IEEE Conference on Computer Communications*, pp. 361–369, April 2014.

[21] S. Depatla, A. Muralidharan, and Y. Mostofi, "Occupancy estimation using only wifi power measurements," *IEEE Journal on Selected Areas in Communications*, vol. 33, pp. 1381–1393, July 2015.

[22] D. Zwillinger, "Crc standard mathematical tables and formulae," 1995.

[23] S. M. Kay, *Fundamentals of Statistical Signal Processing: Estimation Theory*, vol. 1. Prentice Hall, 1993.

[24] H. V. Poor, *An Introduction to Signal Detection and Estimation*. Springer, 2nd edition ed., 1998.

[25] R. L. Graham, D. E. Knuth, and O. Patashnik, *Concrete Mathematics: A Foundation for Computer Science*. Addison-Wesley, 2 edition ed., 1994.

[26] G. Casella and R. L. Berger, *Statistical Inference*. Duxbury Thomson Learning, 2nd edition ed., 2001.

[27] Technical Specification Group Radio Access Network, 3rd Generation Partnership Project, *Spatial Channel Model for Multiple Input Multiple Output (MIMO) Simulations*, 2011. release 10.

[28] H. T. Friis, "A note on a simple transmission formula," *Proceedings of the IRE*, vol. 34, no. 5, pp. 254–256, 1946.

[29] A. Goldsmith, *Wireless Communications*. Cambridge University Press, 2005.

[30] D. Altman, D. Machin, T. Bryant, and M. Gardner, *Statistics with confidence: confidence intervals and statistical guidelines*. John Wiley & Sons, 2013.